Polarization-resolved Second Harmonic microscopy in anisotropic thick tissues

Ivan Gusachenko, Gaël Latour, Marie-Claire Schanne-Klein

Polarization-resolved Second Harmonic microscopy in anisotropic thick tissues

Ivan Gusachenko, Gaël Latour, Marie-Claire Schanne-Klein

Laboratory for Optics and Biosciences, Ecole Polytechnique, CNRS, INSERM U696, 91128 Palaiseau, France

marie-claire.schanne-klein@polytechnique.edu

Abstract: We thoroughly analyze the linear propagation effects that affect polarization-resolved Second Harmonic Generation imaging of thick anisotropic tissues such as collagenous tissues. We develop a theoretical model that fully accounts for birefringence and diattenuation along the excitation propagation, and polarization scrambling upon scattering of the harmonic signal. We obtain an excellent agreement with polarization-resolved SHG images at increasing depth within a rat-tail tendon for both polarizations of the forward SHG signal. Most notably, we observe interference fringes due to birefringence in the SHG depth profile when excited at $\pi/4$ angle from the tendon axis. We also measure artifactual decrease of $\rho = \chi_{xxx}/\chi_{xyy}$ with depth due to diattenuation of the excitation. We therefore derive a method that proves reliable to determine both ρ and the tendon birefringence and diattenuation.

OCIS codes: (180.4315) Nonlinear microscopy; (190.2620) Harmonic generation and mixing; (120.5410) Polarimetry; (170.3660) Light propagation in tissues; (170.6935) Tissue characterization

References and links

1. P. J. Campagnola, A. C. Millard, M. Terasaki, P. E. Hoppe, C. J. Malone, and W. Mohler, "Three-Dimensional High-Resolution Second-Harmonic Generation Imaging of Endogenous Structural Proteins in Biological Tissues," Biophys. J. **82**, 493–508 (2002).
2. W. R. Zipfel, R. Williams, R. Christie, A. Nikitin, B. Hyman, and W. Webb, "Live tissue intrinsic emission microscopy using multiphoton-excited native fluorescence and second harmonic generation." Proc. Natl. Acad. Sci. USA **100**, 7075–7080 (2003).
3. A.-M. Pena, A. Fabre, D. Débarre, J. Marchal-Somme, B. Crestani, J.-L. Martin, E. Beaurepaire, and M.-C. Schanne-Klein, "Three-dimensional investigation and scoring of extracellular matrix remodeling during lung fibrosis using multiphoton microscopy." Microsc. Res. Tech. **70**(2), 162–170 (2007).
4. M. Strupler, M. Hernest, C. Fligny, J.-L. Martin, P.-L. Tharaux, and M.-C. Schanne-Klein, "Second Harmonic Microscopy to Quantify Renal Interstitial Fibrosis and Arterial Remodeling," J. Biomed. Optics **13**, 054041 (2008).
5. S. V. Plotnikov, A. Millard, P. Campagnola, and W. Mohler, "Characterization of the myosin-based source for second-harmonic generation from muscle sarcomeres," Biophys. J. **90**, 328–339 (2006).
6. F. Tiaho, G. Recher, and D. Rouède, "Estimation of helical angle of myosin and collagen by second harmonic generation imaging microscopy," Opt. Express **15**(19), 12286–12295 (2007).
7. A. Deniset-Besseau, J. Duboisset, E. Benichou, F. Hache, P.-F. Brevet, and M.-C. Schanne-Klein, "Measurement of the second order hyperpolarizability of the collagen triple helix and determination of its physical origin." J. Phys. Chem. B **113**(40), 13437–13445 (2009).
8. V. Nucciotti, C. Stringari, L. Sacconi, F. Vanzi, L. Fusi, M. Linari, G. Piazzesi, V. Lombardi, and F. S. Pavone, "Probing myosin structural conformation in vivo by second-harmonic generation microscopy," Proc. Natl. Acad. Sci. USA **107**(17), 7763–7768 (2010).
9. S. Roth and I. Freund, "Second harmonic generation in collagen," J. Chem. Phys. **70**(04), 1637–1643 (1979).

#131579 - $15.00 USD Received 13 Jul 2010; revised 20 Aug 2010; accepted 22 Aug 2010; published 26 Aug 2010

10. P. Stoller, K. Reiser, P. Celliers, and A. Rubenchik, "Polarization-modulated second harmonic generation in collagen," Biophys J. **82**(6), 3330–3342 (2002).
11. P. Stoller, P. Celliers, K. Reiser, and A. Rubenchik, "Quantitative second-harmonic generation microscopy in collagen," Appl. Opt. **42**(25), 5209–5219 (2003).
12. R. Williams, W. R. Zipfel, and W. Webb, "Interpreting second-harmonic generation images of collagen fibrils," Biophys. J. **88**, 1377–1386 (2005).
13. A. Erikson, J. Örtegren, T. Hompland, C. de Lange Davies, and M. Lindgren, "Quantification of the second-order nonlinear susceptibility of collagen I using a laser scanning microscope," J. Biomed. Optics **12**(4), 044002 (2007).
14. X. Han, R. M. Burke, M. L. Zettel, P. Tang, and E. B. Brown, "Second harmonic properties of tumor collagen: determining the structural relationship between reactive stroma and healthy stroma," Opt. Express **16**(3), 1846–1859 (2008).
15. J. C. Mansfield, C. P. Winlove, J. Moger, and S. J. Matcher, "Collagen fiber arrangement in normal and diseased cartilage studied by polarization sensitive nonlinear microscopy," J. Biomed. Optics **13**(4), 044020 (2008).
16. D. Aït-Belkacem, A. Gasecka, F. Munhoz, S. Brustlein, and S. Brasselet, "Influence of birefringence on polarization resolved nonlinear microscopy and collagen SHG structural imaging," Opt. Express **18**(14), 14859–14870 (2010).
17. O. Nadiarnykh, and P. J. Campagnola, "Retention of polarization signatures in SHG microscopy of scattering tissues through optical clearing," Opt. Express **17**, 5794-5806 (2009).
18. M. Strupler, A.-M. Pena, M. Hernest, P.-L. Tharaux, J.-L. Martin, E. Beaurepaire, and M.-C. Schanne-Klein, "Second harmonic imaging and scoring of collagen in fibrotic tissues," Opt. Express **15**(7), 4054–4065 (2007).
19. R. Boyd, *Nonlinear optics* (Academic press, London, 2003).
20. N. J. Kemp, H. N. Zaatari, J. Park, H. G. Rylander, and T. E. Milner, "Form-biattenuance in fibrous tissues measured with polarization-sensitive optical coherence tomography (PS-OCT)," Opt. Express **13**(12), 4611–4628 (2005).
21. J. Park, N. J. Kemp, H. G. Rylander, and T. E. Milner, "Complex polarization ratio to determine polarization properties of anisotropic tissue using polarization-sensitive optical coherence tomography," Opt. Express **17**(16), 13402–13417 (2009).
22. N. Olivier and E. Beaurepaire, "Third-harmonic generation microscopy with focus-engineered beams: a numerical study," Opt. Express **16**(19), 14703–14715 (2008).
23. P. Schön, M. Behrndt, D. Aït-Belkacem, H. Rigneault, and S. Brasselet, "Polarization and phase pulse shaping applied to structural contrast in nonlinear microscopy imaging," Phys. Rev. A **81**(1), 013809 (2010).
24. X. D. Wang, and L. H. V. Wang, "Propagation of polarized light in birefringent turbid media: A Monte Carlo study," J. Biomed. Optics **7**, 279-290 (2002).
25. R. LaComb, O. Nadiarnykh, S. Carey, S. and P. J. Campagnola, "Quantitative second harmonic generation imaging and modeling of the optical clearing mechanism in striated muscle and tendon," J. Biomed. Optics **13**, 021109 (2008).
26. T. Boulesteix, A. Pena, N. Pagès, G. Godeau, M.-P. Sauviat, E. Beaurepaire, and M. Schanne-Klein, "Micrometer scale ex vivo multiphoton imaging of unstained arterial wall structure," Cytometry **69A**(1), 20–26 (2006).

1. Introduction

Second Harmonic Generation (SHG) microscopy is an efficient imaging technique to visualize the three-dimensional (3D) distribution of fibrillar collagen in biological tissues [1, 2]. Incident circular polarization is usually used since it enables imaging of fibrils independently of their orientation in the focal plane. This approach is particularly relevant for quantitative biomedical studies such as fibrosis scoring [3, 4]. However, fibrillar collagen exhibits a structural anisotropy that may be interesting to characterize for many applications. For that purpose, polarization-resolved SHG provides complementary information about the 3D distribution of nonlinear dipoles within the focal volume [5, 6, 7, 8]. The usual approach is to measure the ratio ρ of the two main tensorial components of the nonlinear response, considering a cylindrical symmetry for fibrillar collagen [9, 10, 11, 12, 13, 14]. This ratio depends on the orientational distribution of the collagen triple helices and on the orientation of the nonlinear dipoles (along the peptidic bonds) within the triple helix. ρ therefore provides information about the ordering of collagen molecules or fibrils within the focal volume. It has been measured in various collagenous tissues and showed a wide dispersion of values (1.2 to 2.6). Comparison of healthy and pathological tissue however requires to characterize the accuracy of ρ measure-

#131579 - $15.00 USD Received 13 Jul 2010; revised 20 Aug 2010; accepted 22 Aug 2010; published 26 Aug 2010

ments and their sensitivity to various artifacts. In particular, the anisotropy of many collagenous tissues may affect polarization-resolved SHG experiments as reported in tendons [10, 15, 16]. Polarization-resolved image processing improved when taking into account diattenuation [15] and birefringence [10, 16]. Furthermore, polarization scrambling due to scattering has been shown in tendons and other biological tissues [17].

The aim of this paper is therefore to thoroughly characterize the linear propagation effects that affect polarization-resolved SHG experiments in anisotropic tissues and to develop a reliable method to determine ρ in collagenous tissues. For this purpose, we first develop a theoretical model that fully accounts for birefringence, diattenuation and polarization scrambling upon scattering. We then record polarization-resolved SHG images in rat-tail tendons that is a model tissue composed of aligned collagen fibrils. We finally compare simulated and experimental data that show an excellent agreement and give insight into the linear and nonlinear optical properties of the tendon. Most notably, we observe interference fringes in the SHG depth profiles when excited at $\pi/4$ angle from the tendon axis, and artifactual decrease of ρ with depth due to diattenuation of the excitation. We conclude that the correction for these effects enables a reliable determination of ρ.

2. Experimental setup

2.1. Tendon preparation

Tendons were extracted from Sprague-Dawley rat-tails (female, $\approx$ 300g), centrifugated at 4700 rpm and stored at 4° in phosphate buffer saline (PBS). Imaging was performed within a few days using a water-immersion objective. Tendons were first labelled with fluorescent latex beads to enable precise location of the tissue surface (1μm diameter, L1030, Sigma-Aldrich). After rinsing, they were fixed at both extremities and streched to get rid of the crimps and facilitate alignment of the fibrillar pattern along the *x* direction of the microscope stage. They were kept in PBS on a glass coverslip that maintained them in the focal plane of the microscope.

2.2. Imaging setup

Multiphoton imaging was performed using a custom-built laser scanning microscope [18] as depicted in fig. 1.a. Excitation was provided by a femtosecond Titanium-sapphire laser tuned at 860 nm and scanned in the *xy* directions using galvanometric mirrors. It was focused in the tendon using a water-immersion 20x, 0.95 NA objective that resulted in typically 0.4 µm lateral and 1.6 µm axial resolution near the sample surface. Power was adjusted to 10-15 mW at the focus using a rotating half waveplate and a Glan prism that filtered out *y*-polarization before entering the microscope setup. Nonlinear optical signals were detected using photon-counting photomultiplier tubes and appropriate spectral filters to reject the laser excitation (FF01-680SP, Semrock) and select two-photon excited fluorescence (2PEF) signal (GG455 high-pass filter, Schott) or SHG signal (HQ430/20 interferential filter, Chroma). 2PEF was detected in the backward direction and SHG in the forward direction. Multimodal images were recorded using 100 to 200 kHz pixel rate, 0.4 to 0.8 µm pixel size and 1 to 2 µm*z*-step. They were combined using Matlab and ImageJ softwares as shown in fig. 1.c. Note that there is a slight index mismatch between the tendon ($n = 1.5$) [20] and water ($n = 1.33$), so that the depth *z* within the tendon is related to the lens displacement dz_{lens} by: $z = dz_{lens}\, n_{tendon}/n_{water}$.

2.3. Polarization-resolved measurements

The laser polarization at the back pupil of the objective was approximately along the *x* direction but exhibited a 14% ellipticity due to the optical components within the microscope (9% ellipticity without the dichroic mirror for epi-detection). We therefore inserted an infrared polarizer

#131579 - $15.00 USD Received 13 Jul 2010; revised 20 Aug 2010; accepted 22 Aug 2010; published 26 Aug 2010

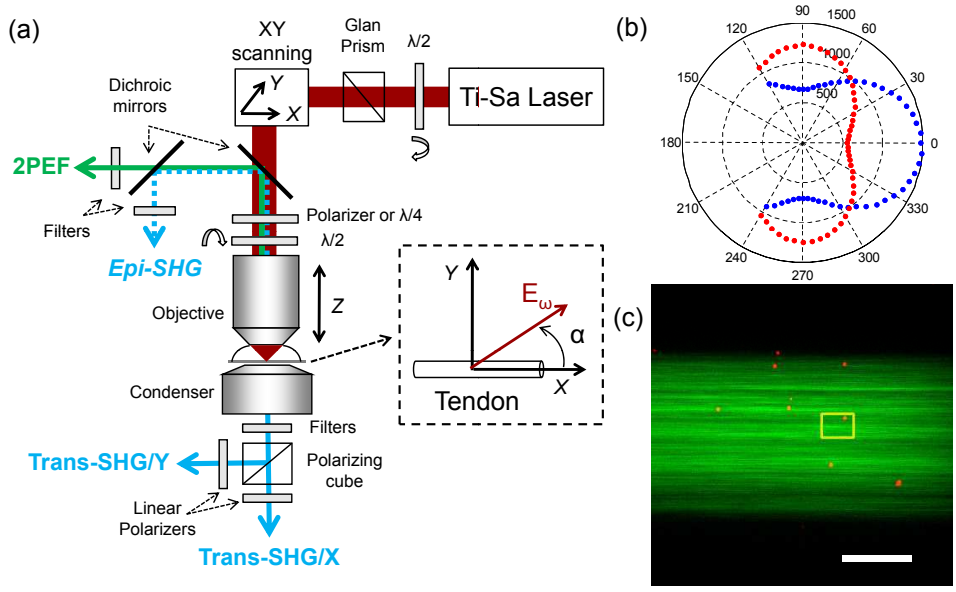

Fig. 1. Experimental setup. (a) Laser scanning multiphoton microscope showing polarization-resolved detection of forward SHG signal and epi-detection of 2PEF signal and possibly of SHG signal. The insert displays the incident electric field relative to the tendon geometry in the focal plane. (b) *x*- and *y*-polarized forward 2PEF signal from a fluorescent slide for variable incident polarization angles. The ratio of the 2 maxima is used for calibration of polarization-resolved SHG signals. (c) Combined 2PEF (red) and SHG (green) image of a tendon labeled with fluorescent latex beads. The image is the summation of 15 images acquired 2µm apart from the tendon upper surface, with enhanced contrast. The yellow box shows a typical Region of Interest used for plotting depth-polar diagrams as in fig. 5. Scale bar: 50µm.

and achieved an ellipcity less than 1% with small scanning angles. This linear polarization was tuned from $-2\pi/3$ to $2\pi/3$ (usually with $\pi/12$ steps) by rotating an achromatic half wave-plate (MWPAA2-22-700-1000, CVI-Melles Griot) placed just before the objective (see fig. 1.a). Forward SHG signals were analyzed using a polarizing beamsplitter cube (BBPC-550, CVI- Melles Griot). To improve the extinction ratio of the *x*- and *y*-polarized detection channels, linear polarizers (03FPG021, CVI- Melles Griot) were set in front of the detectors. The relative transmission of these two channels was calibrated using a fluorescent slide (Chroma): we took advantage of the isotropy of the setup within the *xy* plane and compared the *x*-polarized signal to the *y*-polarized one excited with polarizations shifted by $\pi/2$ angle (see fig.1.b). The ratio of both channels was typically 1.1. Calibration was performed before every experiment and enabled quantitative comparison between *x*- and *y*-polarized signals.

3. Theoretical background

3.1. Polarization-resolved SHG

Let's consider the nonlinear optical interaction of the incident laser beam with a rat-tail tendon. The polarization induced in the medium by the elecric field **E** is given by:

$$P_i = \chi_{ij}^{(1)} E_j + \chi_{ijk}^{(2)} E_j E_k \tag{1}$$

#131579 - $15.00 USD Received 13 Jul 2010; revised 20 Aug 2010; accepted 22 Aug 2010; published 26 Aug 2010

where we considered only the first- and second-order electric susceptibility tensors $\chi^{(1),(2)}$. Rat-tail tendon is commonly assumed to have a cylindrical symmetry (C_{6v} symmetry) [9, 10, 7], which reduces the number of independent nonvanishing $\chi^{(2)}$ components. Moreover, we assume that the Kleinman symmetry is valid as usually considered because of the nonresonant character of the interaction. Within these approximations, there are only 2 independent non-vanishing $\chi^{(2)}$ tensorial components: χ_{xxx} and $\chi_{xyy} = \chi_{xzz} = \chi_{yxy} = \chi_{zxz} = \chi_{yyx} = \chi_{zzx}$, where x represents the main axis of the tendon [19]. Considering a laser beam propagating in the z direction with a linear polarization at angle α to the tendon lying in the xy plane (see fig. 1.a), the electric fields reads: $E_x^\omega = E_0 \cos\alpha$ and $E_y^\omega = E_0 \sin\alpha$ near the focus and induces a SH polarization:

$$\begin{aligned} P_x^{2\omega} &\propto \left(\chi_{xxx}\cos^2\alpha + \chi_{xyy}\sin^2\alpha\right) E_0^2 \\ P_y^{2\omega} &\propto \left(\chi_{xyy}\sin 2\alpha\right) E_0^2 \end{aligned} \tag{2}$$

which radiates at frequency 2ω. In this paper, we are interested in ratiometric measurement of the second-order response and we consider the ratio of the two independent tensorial components of the second-order susceptibility: $\rho = \chi_{xxx}/\chi_{xyy}$. This ratio provides insight into the orientational distribution of the collagen molecules within the focal volume. It is taken to be real in the Kleiman approximation. The SH intensity detected for each polarisation then reads:

$$I_x^{2\omega} = K\left|\rho\cos^2\alpha + \sin^2\alpha\right|^2 \tag{3a}$$

$$I_y^{2\omega} = K\left|2\sin\alpha\cos\alpha\right|^2 \tag{3b}$$

where K is a constant merging various parameters such as setup geometry and squared incident beam intensity I_0^2. Polar diagrams of eq. (3) are displayed in fig. 2.a and b using $\rho = 1.4$. A common method to determine ρ from polarization-resolved SH experiments is to fit $I_x^{2\omega}$ using eq. (3*a*).

In the following, we propose a more general method. Since $I_x^{2\omega}$ and $I_y^{2\omega}$ are even functions of α and contain only even powers of trigonometric functions, they can be represented as a sum of $\cos 2n\alpha$ functions:

$$I_x^{2\omega} = A\cos 4\alpha + B\cos 2\alpha + C \tag{4a}$$

$$I_y^{2\omega} = \frac{K}{2}\left(-\cos 4\alpha + 1\right) \tag{4b}$$

where

$$A = \frac{K}{2}\left(\frac{\rho-1}{2}\right)^2 \tag{5a}$$

$$B = 2K\left(\frac{\rho-1}{2}\right)\left(\frac{\rho+1}{2}\right) \tag{5b}$$

$$C = \frac{K}{2}\left(\frac{\rho-1}{2}\right)^2 + K\left(\frac{\rho+1}{2}\right)^2 \tag{5c}$$

In that framework, one can notice that:

$$\rho^2 = \frac{A+B+C}{A-B+C} \tag{6}$$

This expression enables the determination of ρ from polarization-resolved SH data by fitting $I_x^{2\omega}$ using eq. (4*a*). The advantage of this method is that it can take into account various physical effects that appear to modify the expression of $I_x^{2\omega}$ but not its representation as a sum of $\cos 2n\alpha$ functions. These physical effects will be presented in the following sections and the new expressions of the A, B and C parameters will be derived.

#131579 - $15.00 USD Received 13 Jul 2010; revised 20 Aug 2010; accepted 22 Aug 2010; published 26 Aug 2010

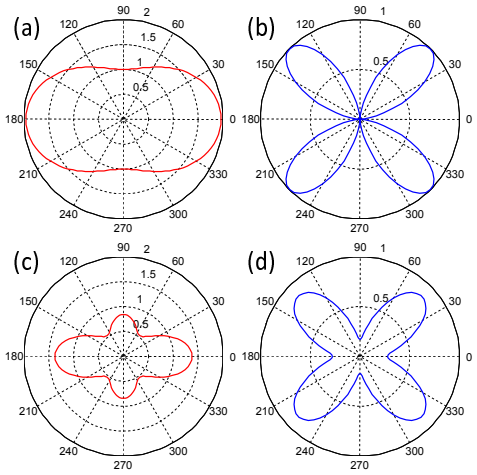

Fig. 2. Simulated polar diagrams of polarization-resolved SH intensity generated by a tendon aligned along x axis. The angle represents the direction of the excitation polarization to the tendon direction (see fig. 1.a). (a) $I_x^{2\omega}$ and (b) $I_y^{2\omega}$ in a non-birefringent, non-scattering medium without diattenuation (see eq. (2)). (c) $I_x^{2\omega}$ and (d) $I_y^{2\omega}$ at 24µm depth considering birefringence (Δn = 0.0066), diattenuation (Δl_a = 175µm) and polarisation cross-talk due to scattering ($\eta_{xy} = 0.13$) (see Eq. (11)). $\rho = 1.40$ in all simulations.

3.2. Tendon birefringence

In the former derivation of $I^{2\omega}$, we have assumed that the electric field propagation takes place in an isotropic medium. Nevertheless, the tendon is considered to exhibit a C_{6v} symmetry, so that the permittivity tensor $\varepsilon_0\left(1+\chi_{ij}^{(1)}\right)$ has two different components and the tendon is analogous to a uniaxial birefringent crystal. Indeed, it has been reported that birefringence $\Delta n = n_e - n_o$ attains $5\cdot 10^{-3}$ [20, 21] in tendon. As a consequence, the x (extraordinary wave) and y (ordinary wave) excitation field components undergoes a relative phase retardation when propagating within the tendon. SH intensity then reads:

$$I_x^{2\omega}(z) = K\left|\rho\cos^2\alpha e^{i\Delta\phi} + \sin^2\alpha\right|^2 = K\left(\left|\rho\cos^2\alpha+\sin^2\alpha\right|^2 + \frac{\rho}{2}\sin^2 2\alpha\left(\cos\Delta\phi - 1\right)\right) \quad (7a)$$

$$I_y^{2\omega}(z) = K\left|sin2\alpha\; e^{i\frac{2\pi(n_e+n_o)}{\lambda}z}\right|^2 = K\left|sin2\alpha\right|^2 \quad (7b)$$

where $\Delta\phi = \frac{4\pi(n_e-n_o)z}{\lambda}$ accounts for the birefringence in the excitation propagation (SHG intensity is unaffected by birefringence in the harmonic propagation). Note that z represents the depth in tendon at which SH takes place: due to index mismatch, $z = dz_{lens}\, n_{tendon}/n_{water}$, where dz_{lens} is the microscope lens displacement from the tendon upper surface.

These expressions show that $I_y^{2\omega}$ is unaffected by birefringence, while $I_x^{2\omega}$ has a supplemen-

#131579 - $15.00 USD Received 13 Jul 2010; revised 20 Aug 2010; accepted 22 Aug 2010; published 26 Aug 2010

tary term compared to eq. (4). Decomposing $I_x^{2\omega}$ in the $\cos 2n\alpha$ basis, we get:

$$A_{biref} = K\left[\frac{1}{2}\left(\frac{\rho-1}{2}\right)^2 + \frac{\rho}{4}(1-\cos\Delta\phi)\right] \tag{8a}$$

$$B_{biref} = 2K\left(\frac{\rho-1}{2}\right)\left(\frac{\rho+1}{2}\right) \tag{8b}$$

$$C_{biref} = K\left[\frac{1}{2}\left(\frac{\rho-1}{2}\right)^2 + \left(\frac{\rho+1}{2}\right)^2 - \frac{\rho}{4}(1-\cos\Delta\phi)\right] \tag{8c}$$

One observes that $B_{biref} = B$ and $A_{biref} + C_{biref} = A + C$, so that ρ can be determined using eq. 6 as in section 3.1. To get better insight into the effect of birefringence, we have plotted in fig. 3 the variation of $I_x^{2\omega}$ and $I_x^{2\omega}$ as a function of the incident polarization angle α for increasing depth within the tendon. Comparison of model calculations with and without birefringence shows that birefringence results in interference fringes in the *x*-polarized SH intensity $I_x^{2\omega}$ when excited with a linear polarization at $\pi/4$ from the tendon axis, as shown by the $\cos\Delta\phi$ term in eq. 7a (see *z*-profiles in 3.k and 3.n).

3.3. Polarization cross-talk

We have assumed yet that propagation occurs in an optically perfect medium. However, tendon is a scattering medium like most biological tissues. It results in the decrease of the excitation intensity since scattered light is not intense enough to induce a nonlinear response. This effect, that may be different for *x*- and *y*-polarized incident light, will be considered in the next section. Here, we are interested in the effect of light scattering on the harmonic beam polarization. When propagating in an anisotropic scattering medium, a wave with well-defined polarization accumulates scrambling over its polarization direction since scattering processes slightly rotate the polarization direction. As a consequence, a small amount of SH light that is initially polarized along *y* is detected in the *x*-polarized channel and vice versa. Let η_{XY} (resp. η_{YX}) be the amount of that polarization "cross-talk" from *y* detection channel to *x* detection channel (resp. from *x* to *y*), so $I^{2\omega}$ reads:

$$I_x^{2\omega}(z) = K\left|\rho\cos^2\alpha + \sin^2\alpha\right|^2 + \eta_{XY}K\left|sin2\alpha\right|^2 \tag{9a}$$

$$I_y^{2\omega}(z) = \eta_{YX}K\left|\rho\cos^2\alpha + \sin^2\alpha\right|^2 + K\left|sin2\alpha\right|^2 \tag{9b}$$

Decomposing $I_x^{2\omega}$ in the $\cos 2n\alpha$ basis, we obtain:

$$A_{pol} = K\left[\frac{1}{2}\left(\frac{\rho-1}{2}\right)^2 - \frac{\eta_{XY}}{2}\right] \tag{10a}$$

$$B_{pol} = 2K\left(\frac{\rho-1}{2}\right)\left(\frac{\rho+1}{2}\right) \tag{10b}$$

$$C_{pol} = K\left[\frac{1}{2}\left(\frac{\rho-1}{2}\right)^2 + \left(\frac{\rho+1}{2}\right)^2 + \frac{\eta_{XY}}{2}\right] \tag{10c}$$

Once again, $B_{pol} = B$ and $A_{pol} + C_{pol} = A + C$, and ρ can be determined as before. Fig. 3.b and g show that the angular profiles of $I_x^{2\omega}$ and $I_y^{2\omega}$ are slightly modified by polarization cross-talk.

3.4. Diattenuation in tendon

Multiphoton microscopy uses near-infrared excitation which minimizes absorbance and scattering in biological tissues. Nevertheless, light scattering and spherical aberrations cause focal

#131579 - $15.00 USD Received 13 Jul 2010; revised 20 Aug 2010; accepted 22 Aug 2010; published 26 Aug 2010

volume deterioration upon propagation within the tendon, which results in smaller excitation intensity and weaker SH signal. For simplicity, we assume that the excitation intensity undergoes exponential attenuation with depth. Due to the tendon anisotropy, the effective attenuation lengths for I_x^ω and I_y^ω are different and the excitation light experiences diattenuation. These attenuation lengths will be noted as l_a^e and l_a^o to account for the uniaxial symmetry of the tendon. We assume that diattenuation of the SH signal is negligible because signal forward-detection in multiphoton setups is not much sensitive to light scattering and aberrations. $I_{x,y}^{2\omega}$ then reads:

$$I_x^{2\omega}(z) = K\left|\rho\cos^2\alpha e^{-\frac{z}{l_a^e}} + \sin^2\alpha e^{-\frac{z}{l_a^o}}\right|^2 = Ke^{-\frac{2z}{l_a^o}}\left|\rho e^{-\frac{z}{\Delta l_a}}\cos^2\alpha + \sin^2\alpha\right|^2 \quad (11a)$$

$$I_y^{2\omega}(z) = K\left|sin2\alpha\, e^{-\frac{z}{2l_a^o}} e^{-\frac{z}{2l_a^e}}\right|^2 = Ke^{-\frac{2z}{l_a^o}} e^{-\frac{z}{\Delta l_a}}\left|sin2\alpha\right|^2 \quad (11b)$$

where $\frac{1}{\Delta l_a} = \frac{1}{l_a^e} - \frac{1}{l_a^o}$. The expression of the A, B and C parameters are the same as in eq. 5 with the modified parameters: $K \to Ke^{-\frac{2z}{l_a^o}}$ and $\rho \to \rho e^{-\frac{z}{\Delta l_a}}$. Consequently, once Δl_a is known, ρ can be determined in a similar way as in section 3.1. Note that this approach can be generalized to an arbitrary diattenuation profile $f_a(z) = f_a^x(z)/f_a^y(z)$ by using the transformation $\rho \to \rho f_a(z)$ in eq. 6. Fig. 3.c, h and m show the modifications of $I_x^{2\omega}$ and $I_y^{2\omega}$ induced by diattenuation. In particular, z-profiles for an incident polarization parallel (resp. perpendicular) to the tendon exhibit a l_a^e (resp. l_a^o) exponential decay.

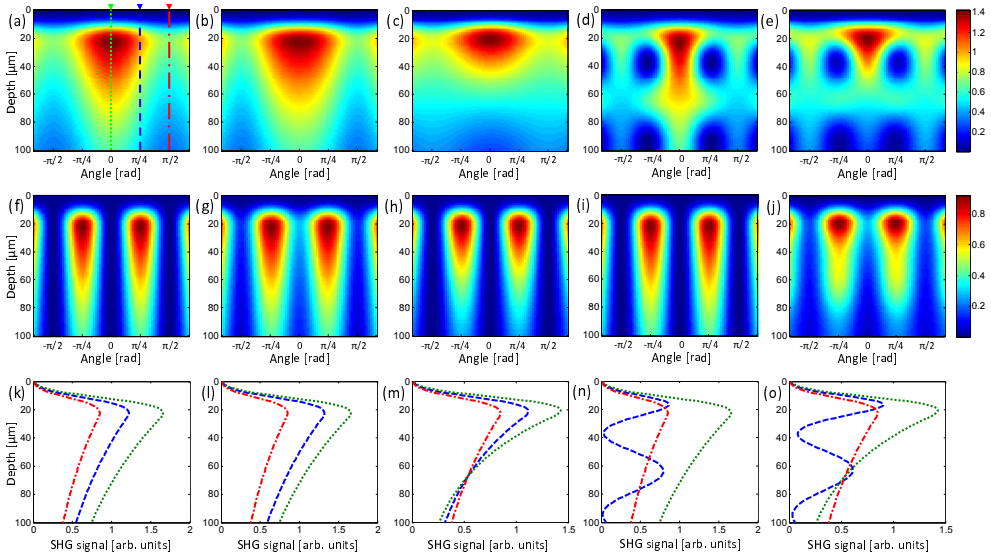

Fig. 3. Numerical calculation of polarization-resolved SH intensity as a function of incident polarisation angle α (see fig. 1) and depth z within tendon for different parameters. (a)-(e) $I_x^{2\omega}$, (f)-(j) $I_y^{2\omega}$ and (k)-(o) z-profiles of $I_x^{2\omega}$ for $\alpha = 0$ (green dotted line), $\alpha = \pi/4$ (blue dashed line) and $\alpha = \pi/2$ (red dash-dot line). (a), (f), (k) tendon with uniform depth-attenuation: $l_x^a = l_y^a = 190\mu$m. (b), (g), (l) tendon with polarization cross-talk: $\eta_{xy} = 0.13$, $\eta_{yx} = 0.2$ (constant with depth). (c), (h), (m) tendon with diattenuation: $l_a^e = 91\mu$m and $l_a^o = 190\mu$m. (d), (i), (n) tendon with birefringence $\Delta n = 0.0066$. (e), (j), (o) tendon with diattenuation, birefringence and polarisation cross-talk (same parameters). ρ is equal to 1.40 for all calculations.

#131579 - $15.00 USD Received 13 Jul 2010; revised 20 Aug 2010; accepted 22 Aug 2010; published 26 Aug 2010

3.5. *Combined effects of birefringence, polarization cross-talk and diattenuation*

When taking into account all the effects introduced above, we obtain the following expression:

$$I_x^{2\omega}(z) = Ke^{-\frac{2z}{l_a^o}}\left(\left|\rho e^{-\frac{z}{\Delta l_a}}\cos^2\alpha e^{i\Delta\phi} + \sin^2\alpha\right|^2 + \eta_{XY}e^{-\frac{z}{\Delta l_a}}\left|sin2\alpha\right|^2\right) \tag{12}$$

Fig. 2.c and d display the polar diagrams of this expression along with the similar expression for $I_y^{2\omega}$. They clearly look very different from the polar diagrams a and b plotted from the simplified model (eq. 3). It shows that determination of ρ using eq. 3a is hazardous. Conversely, $I_x^{2\omega}$ can still be decomposed as a sum of $\cos 2n\alpha$ functions as in eq. 4a: the parameters A_{eff}, B_{eff} and C_{eff} are obtained by combining the effects of birefringence (eq. 8) and polarization cross-talk (eq. 10) only, and considering the modified parameters: $K \rightarrow Ke^{-\frac{2z}{l_a^o}}$, $\rho \rightarrow \rho e^{-\frac{z}{\Delta l_a}}$ and $\eta_{xy} \rightarrow \eta_{xy}e^{-\frac{z}{\Delta l_a}}$. In that framework, ρ can be determined as follows:

$$\rho^2 e^{\frac{-2z}{\Delta l_a}} = \frac{A_{eff}+B_{eff}+C_{eff}}{A_{eff}-B_{eff}+C_{eff}} \tag{13}$$

given that z-profiles of $I_x^{2\omega}$ for $\alpha = 0$ and $\frac{\pi}{2}$ can be used to determine l_a^e and l_a^o (or $f_a(z)$ in a more general case).

The right hand side of fig. 3 displays the x- and y-polarized SH signal given by eq. 12: diattenuation is revealed by differences in z attenuation for incident polarization parallel and perpendicular to the tendon axis, birefringence by oscillations in the z-profile at $\pi/4$ polarization angle from the tendon axis and polarization cross-talk by deformation of the angular profiles. In order to better evidence the latter two effects, we introduce the parameter Δ that sorts out the contributions of $\Delta\phi$ and η_{XY} to A_{eff} and C_{eff}:

$$\Delta(z) = \frac{C-3A-\sqrt{(A+C)^2-B^2}}{2(A-B+C)} \tag{14a}$$

$$\Delta(z) = f_a\left[\eta_{XY} - \frac{\rho}{2}(1-\cos\Delta\phi)\right] \tag{14b}$$

At a given depth, contributions of birefringence and polarization cross-talk are intrinsically mixed, but information on these effects can be obtained by analysis of Δ depth variation.

4. Results

Fig. 4 displays typical x- and y-polarized SHG images obtained at various depths within a tendon for an incident beam polarized at $\pi/4$ from the tendon axis. Transverse profiles show that the SHG signal is higher at the tendon edges as expected because of the cylindrical shape of the tendon: attenuation of the excitation beam is more effective in the center of the section when the incident light propagates along a larger distance within the tendon. However, the x- and y-polarized SHG transverse profiles exhibit different behaviour as a function of the depth from the tendon upper surface. In fig. 4.a and b, the x-polarized SHG image is more attenuated than the y-polarized SHG image at the tendon center, whereas it is not the case in fig. 4.c and d. Moreover, the x-polarized SHG image at 57µm (fig. 4.c) displays more signal at the center than at intermediate positions along the transverse profile. This complex behaviour is characteristic for birefringence effects. The x and y components of the $\pi/4$-polarized incident beam experience different optical indices when propagating within the tendon and accumulate a relative phase shift. The tensorial components of the nonlinear response excited by the x and y components of the $\pi/4$-polarized incident beam then interfere in a constructive or destructive

#131579 - $15.00 USD Received 13 Jul 2010; revised 20 Aug 2010; accepted 22 Aug 2010; published 26 Aug 2010

way, depending on the propagation distance within the tendon. It results in interference fringes in the depth profile of the SHG signal for incident excitation mixing up x and y-polarization components. These fringes appear only in x-polarized SHG images because they result from the coherent summation of two tensorial components excited along x and y polarizations respectively (see eq. 2). Conversely, y-polarized SHG images are not sensitive to birefringence because they probe only one tensorial component.

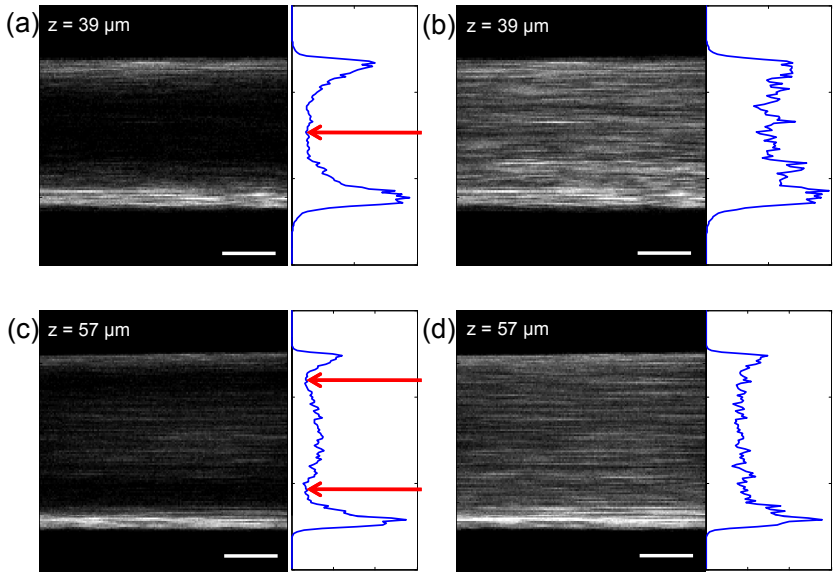

Fig. 4. Polarization-resolved SH images of a tendon upon excitation polarized at $\pi/4$ from the tendon axis. (a)-(c) x- and (b)-(d) y-polarized SH images and transverse profiles of a tendon aligned along x axis at (a)-(b) 39 µm depth and (c)-(d) at 57 µm depth from the tendon upper surface. x-polarisation images shows dark fringes (red arrows), whereas y-polarisation has almost uniform intensity profile in the tendon center. Scale bar: 50 µm.

To get a better insight into the physics of polarization-resolved SHG images, we carried out SHG experiments at increasing depth within the tendon. Fig. 5.a and b display typical x- and y-polarized SHG signals in 28 x 20µm regions of interest such as the one depicted in fig. 1.a. The depth profile of the 2PEF signal from the latex beads is also displayed in fig. 5.c. It enables the location of the tendon surface z_0 that corresponds to the maximum of the 2PEF peak. The specific patterns observed in the SHG images were consistently observed in all our samples provided that the ellipticity of the incident polarization was negligible. Practically, experiments performed without a linear polarizer at the back pupil of the objective lens exhibited a non symmetrical pattern relative to the tendon axis ($\alpha = 0$).

Fig. 5.f displays z-profiles of the x-polarized SHG signal for various incident polarization angles. Interference fringes characteristic for birefringence in the excitation propagation are clearly observed for an incident polarization at $\pi/4$ angle to the tendon axis. The distance between the two maxima is $\delta z \approx 47$µm. In a first approximation, it is related to the birefringence phase shift by $\Delta n = \lambda/2\delta z$. It gives: $\Delta n \approx 0.008$ (after index mixmatch correction), in qualitative agreement with reported birefringence in tendon [20, 21]. It will be determined more precisely later on. Diattenuation of the laser excitation is suggested by the z-profiles of the x-polarized SHG signal at 0 and $\pi/2$ angles. Exponential fitting gives the following attenuation

#131579 - $15.00 USD Received 13 Jul 2010; revised 20 Aug 2010; accepted 22 Aug 2010; published 26 Aug 2010

lengths for x and y incident polarizations : $l_a^e = 91\mu m$ and $l_a^o = 190\mu m$ (see fig. 6.a).

Finally, fig. 5.d and e display $I_x^{2\omega}$ and $I_y^{2\omega}$ at the surface of the tendon ($z = z_0$) where birefringence and diattenuation effects do not apply. We therefore fit our data using eq. 9 that accounts only for polarization cross-talk due to light scattering (or equivalently, using eq. 12 with $z = 0$ and $\Delta\phi = 0$). We observe that the experimental data are better fitted using eq. 9 than in the simplified approach (eq. 3). It shows that polarization cross-talk due to light scattering significantly distorts the polarization pattern at the tendon surface.

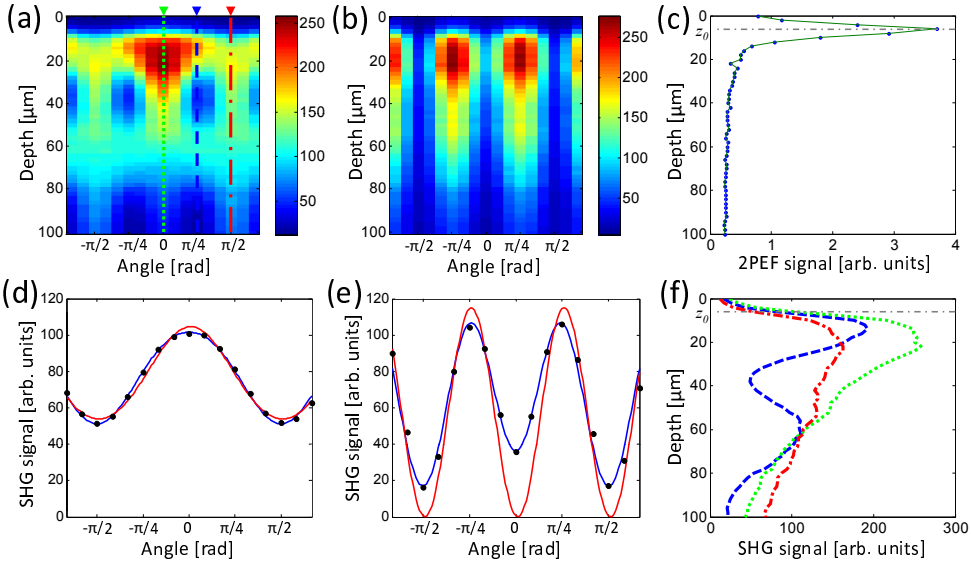

Fig. 5. Experimental polarization-resolved SH intensity from a tendon. (a) $I_x^{2\omega}$ and (b) $I_y^{2\omega}$ as a function of incident polarisation angle α (see fig. 1) and lens displacement. (c) z-profile of fluorescence signal from latex beads, peaking at the tendon surface z_0. (d) $I_x^{2\omega}(\alpha)$ and (e) $I_y^{2\omega}(\alpha)$ at the tendon surface (black dots), along with fits using the simplified approach (eq. 3, red line) or accounting for polarization cross-talk (eq. 9, blue line). (f) experimental z-profiles of $I_x^{2\omega}$ for $\alpha = 0$ (green dotted line), $\alpha = \pi/4$ (blue dashed line) and $\alpha = \pi/2$ (red dash-dot line).

Altogether, these experimental observations show that the usual approach with eq. 3 does not satisfactorily account for polarization-resolved SHG imaging in thick tendons. Birefringence, diattenuation and polarization cross-talk due to scattering must all be taken into account to explain experimental data. Accordingly, we used eq. 4 with parameters A_{eff}, B_{eff} and C_{eff} to fit our data. Note that we introduced an angular shift α_0 to account for possible slight misalignment of the tendon axis from x direction ($-2^\circ < \alpha_0 < 2^\circ$ for all our data). We then calculated $\rho e^{\frac{-z}{\Delta l_a}}$ by use of eq. 13. This value was subsequently corrected for diattenuation using $l_a^e = 91\mu m$ and $l_a^o = 190\mu m$ obtained from exponential fitting of $I_x^{2\omega}(\alpha = 0)$ and $I_x^{2\omega}(\alpha = \pi/2)$. Both the raw and corrected values of ρ are depicted in fig. 6.b. Diattenuation correction successfully removes the artifactual variation of ρ with depth and enables the reliable determination of this parameter: $\rho = 1.40 \pm 0.03$. Moreover, as already stated, this approach is applicable to any attenuation profile $f_a(z)$. To fully characterize the optical response of our sample, we also calculated the parameter $\Delta(z)$ from eq. 14a and plotted its depth profile in fig. 6.c. Eq. 14b shows that the values at the maxima ($\Delta\phi = 2\pi k$ with k integer) reduce to η_{xy}. The first maximum is obtained at the tendon surface: $\eta_{xy} = 0.13$. The second maximum is zero which shows that

#131579 - $15.00 USD Received 13 Jul 2010; revised 20 Aug 2010; accepted 22 Aug 2010; published 26 Aug 2010

$e^{\frac{-z}{\Delta l_a}}\eta_{xy}$ is negligible $\approx 60\mu$m deep within the tendon. We then consider that η_{xy} diminishes exponentionally from 0.13 to 0 within the first 40µm from the surface and we get $\Delta n = 0.0066$ by fitting our data using eq. 14b ($\Delta n = 0.0074$ without any index mismatch correction).

Finally, to verify the consistency of our data processing, let's compare our experimental data (fig. 5.a and b) to the simulations using our experimentally determined parameters for birefringence, diattenuation and polarization cross-talk (fig. 3.e and j). The theoretical and experimental intensity maps are in excellent agreement which proves that our theoretical approach satisfactorily reproduces polarization-resolved SHG experiments in tendons.

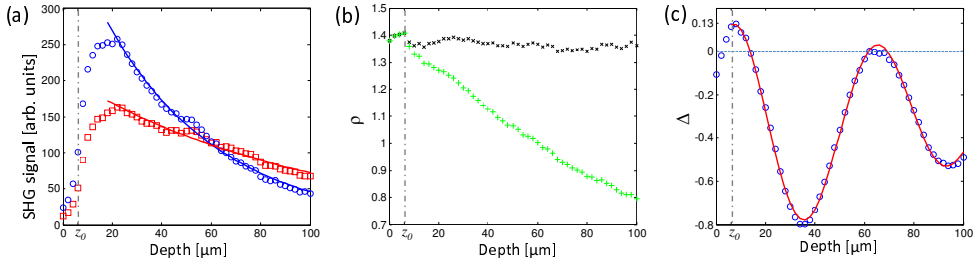

Fig. 6. Determination of tendon characteristic parameters from experimental SH depth-profiles. (a) $I_x^{2\omega}(\alpha = 0)$ (blue dots) and $I_x^{2\omega}(\alpha = \pi/2)$ (red squares) showing diattenuation: the solid lines correspond to exponential fitting with $l_a^e = 91\mu$m and $l_a^o = 190\mu$m. (b) ρ determined from polarization-resolved SHG measurements with (black) and without (green) correction for diattenuation. (c) Δ parameter evidencing birefringence (oscillations), polarization cross-talk due to scattering (non-vanishing value at the tendon surface) and diattenuation (exponential attenuation with depth). The solid line represents fitting with the following parameters: $\Delta n = 1.40$, $\eta_{xy} = 0.13$ near the surface and $\Delta l_a = 134\mu$m.

5. Discussion

In this paper, we developed a method to account for linear propagation effects affecting the polarization when determining ρ by polarization-resolved SHG experiments. Previous works studied the effects of diattenuation [15] and birefringence [10, 16] separately, but they did not propose an approach accounting for both effects and enabling the determination of ρ at any depth. Our model considers birefringence and diattenuation along the excitation beam propagation and polarization cross-talk due to scattering of the SHG signal. Our experimental results show that this model perfectly fits our data on rat-tail tendons and enables the reliable determination of ρ. We also observed interference fringes in the SHG depth profiles which show unambiguously that birefringence affects polarization-resolved SHG microscopy. Our model may be refined by numerical simulations of the field distribution within the focal volume using a vectorial approach to properly describe the polarizations [22]. Such a calculation would account for polarization mixing through the high numerical aperture objective lens [22, 23] and for deformation of the focal volume due to birefringence. The description of the polarization may also be further refined by using Mueller matrices and tracking Stokes vectors through the tendon [24]. The advantage of our model however is to include all the characteristic features of the biological sample in a phenomenological approach, including light scattering or depolarization. It presumably explains why it shows an excellent agreement with our experimental data and proves relevant to determine optical parameters of rat-tail tendon.

Our data gives insight into both the linear and nonlinear optical response of the tendon. It first enables the determination of the tendon birefringence at the excitation wavelength. We obtain $\Delta n = 6.6\ 10^{-3}$ in good agreement with recently reported values measured in a more

#131579 - $15.00 USD Received 13 Jul 2010; revised 20 Aug 2010; accepted 22 Aug 2010; published 26 Aug 2010

direct way using Optical Coherence Tomography (OCT) ($\Delta n = 5.3\ 10^{-3}$) [20, 21]. We also measure the diattenuation at 860*nm*, $\Delta l_a = 175\mu$m, and the polarization cross-talk due to scattering, $\eta_{xy} = 13\%$. Our measured values seem reasonable considering usual optical properties in biological tissues. Previous work also reported polarization scrambling in tendon that could be reduced by optical clearing [17]. Our phenomenological parameter $\eta_{xy} = 13\%$ amounts to an average SHG polarization rotation of about 20°. It shows that the SHG polarization is reasonably well preserved in the forward direction although propagation to the detector takes place over several scattering lengths. Indeed, forward detection picks up mainly quasi-ballistic photons and the polarization of these photons is not strongly modified. Similarly, the measured attenuation lengths ($l_a^e = 91\mu$m and $l_a^o = 190\mu$m) are in good agreement with our previous measurements in rat-artery [26] and the diattenuation shows qualitative agreement with previously reported measurements in rat-tail tendon using OCT ($\Delta l_a = 125\mu$m [20, 21]) or in horse flexor tendon using SHG microscopy ($\Delta l_a = 480\mu$m [15]). Note that the precise determination of these parameters depends on the tendon index considered for index mismatch correction. Finally, as intended from these polarization-resolved SHG experiments, they determine the ratio ρ of the two main tensorial components of the tendon second-order susceptibility. We obtain $\rho = 1.40 \pm 0.03$ from the experimental data displayed in fig. 5. Similar values in the range 1.3 to 1.5 were consistently obtained in all our samples. The reproducibility of these measurements is excellent considering the dispersion of tissue properties in biological samples. Slight differences from one tendon to the other may moreover be attributed to differences in the tendon preparation, particularly in the tendon stretching, that could affect the 3D distribution of fibrils at a submicrometric scale.

Most importantly, our measurements show that the raw value of ρ varies a lot with depth as depicted in fig. 6.b. It decreases from 1.40 at the surface of the tendon to 0.8 at $\approx 90\mu$m depth within the tendon. These data proves that correction for diattenuation is essential for reliable measurements of ρ in thick anisotropic tissues and that our model provides an efficient correction along the full stack of data. We expect that the determination of ρ deeper in the tissue would be hampered because of the low signal to noise ratio. When possible, the most reliable method is to perform polarization-resolved measurements at the sample surface to get rid of diattenuation and birefringence effects.

Finally, note that this method is also applicable to epidetected SHG signals. In that configuration, the infrared polarizer set before the half waveplate at the back pupil of the objective has to be replaced by a quarter waveplate set at a suitable angle to correct for incident ellipticity without rejecting some epi-SHG signal (see fig. 1.a). Polarization analysis of this epidetected SHG signal is a complex task because of the presence of the waveplates. Furthermore, backward-detected SHG is highly affected by scattering and related polarization distortion [25, 17]. However, SHG polarization analysis was required here for properly characterizing the different linear optical effects that may affect the determination of ρ. Once this study is completed, the total SHG intensity can be fitted like the *x*-polarized component as a sum of $\cos 2n\alpha$ functions, using an expression similar to eq. 12. Favourably, this configuration does not require the alignment of the tendon axis relative to polarization analysis.

6. Conclusion

In this paper, we combined model calculation and experiments in rat-tail tendon to characterize linear optical effects that affect the polarization in polarization-resolved SHG experiments. We evidenced that birefringence, diattenuation and polarization scrambling upon scattering significantly distort the SHG response for tunable incident linear polarizations. In particular, birefringence results in interference fringes in the depth profile of the SHG signal excited with polarization at $\pi/4$ angle from the tendon axis. Most importantly, diattenuation results in an ar-

#131579 - $15.00 USD Received 13 Jul 2010; revised 20 Aug 2010; accepted 22 Aug 2010; published 26 Aug 2010

tifactual decrease of ρ with the depth within the tendon. To address these problems, we derived a method to process polarization-resolved SHG data and we successfully retrieved relevant optical parameters in rat-tail tendon. This method is applicable to any anisotropic sample that exhibits SHG signals, including other collagenous tissues and presumably skeletal muscles. It may also be generalized to other nonlinear optical processes, that is 2PEF, THG, CARS or SRS polarization-resolved microscopies. Altogether, our work proves unambiguously that uncorrecting for polarization distortion results in misleading determination of the tensorial nonlinear response in anisotropic thick tissues.

Acknowledgements

We gratefully acknowledge G. Liot from Institut Curie, Université Paris XI, for providing us with the rat-tails, X. Solinas and J.-M. Sintès for technical implementation of the setup, A. de Martino, E. Beaurepaire and D. Débarre for fruitful discussions, and F. Hache for critical reading of this manuscript. G. Latour was supported by RTRA-Triangle de la Physique.

#131579 - $15.00 USD Received 13 Jul 2010; revised 20 Aug 2010; accepted 22 Aug 2010; published 26 Aug 2010